

Self-Diagnosis and Self-Repair of an Active Tensegrity Structure

Bernard Adam, Ph.D.¹ and Ian F. C. Smith, F.ASCE²

Abstract: This paper focuses on the study of tensegrity active control in situations of partially defined loading and damage events. Self-diagnosis and self-repair methodologies are proposed and validated experimentally on a full-scale active tensegrity structure. Self-diagnosis involves load identification and damage location. The response of the structure to a load and damage is measured and compared with the response of the structure to candidate solutions for load and damage. Self-diagnosis solutions result in sets of candidate solutions for loads and damage. These solutions are employed to compute control commands of shape control and self-repair for the structure. Self-repairing control commands increase stiffness and decrease stresses with respect to the damaged state. Self-repairing control commands are computed using a multiobjective approach. The application of a control command results in self-stress modifications by changing the length of active struts. The proposed methodologies are attractive for tensegrity active control in situations of partially defined loading and damage events.

DOI: 10.1061/(ASCE)0733-9445(2007)133:12(1752)

CE Database subject headings: Space structures; Structural control; Diagnosis; Adaptive systems; Nonlinear response.

Introduction

Most civil engineering structures are passive and static. While they deflect in a passive manner, they do not adapt actively to external loading. A more challenging functionality of civil engineering structures is that they react and adapt actively to changing requirements, such as new loading and eventual damage. Shea et al. (2002) presented a computational framework based on intelligent control methodology that combines reasoning from explicit knowledge, search, learning, and planning to illustrate a vision of intelligently controlled civil engineering structures.

While adaptive structures are an emerging research topic in civil engineering, bio-inspired systems have already been studied in domains such as mathematics, electronics, and informatics. In mathematics, Von Neumann (1966) proposed an automaton that could self-repair and self-reproduce. Teuscher et al. (2003) studied a fault-tolerant "Bio-Watch" that exhibited self-repairing characteristics and interacted with its environment. In computer science, Sterritt et al. (2005) postulated that autonomic computing systems are useful since they continue to be useful as conditions change. However, these examples come from virtual worlds of information science, whereas civil engineering structures exist in the physical environment.

In structural engineering, Sobek and Teuffel (2002) performed numerical studies on the control of lightweight structures that react to external stimuli, such as varying loadings and noise. Pawlowski and Holnicki-Szulc (2004) introduced a structure that could adapt to extreme loads. It detected impacts through a set of sensors and optimally distributed forces in the structure using structural fuses. However no experimental study has demonstrated self-diagnosis and self-repair in civil engineering structures.

Since tensegrities can be equipped with active control systems, they have the potential to adapt to partially defined environments. Tensegrities are spatial, reticulated, and lightweight structures. These structures are composed of struts and tendons. Stability is provided by the self-stress state between a tensioned cable net and compressed strut elements (Motro 1984). A recent and widely accepted definition has been proposed by Motro (2003): "A tensegrity system is a system in a stable self-equilibrated state comprising a discontinuous set of compressed components within a continuum of tensioned components."

Few studies have focused on tensegrity control. Kawaguchi et al. (1996) studied shape and stress control of prestressed truss structures. Difficulties were identified in validating numerical results through experimental testing. Averseng and Crosnier (2004) studied the control of a tensegrity grid in which the actuation system is connected to the supports.

Fest et al. (2004) demonstrated experimentally the feasibility of tensegrity active shape control. The most challenging part of the study was the computation of control commands (sequence of contractions and elongations of active struts) that modify the self-stress state in order to recover the top surface slope of the structure when subjected to a load. Since the behavior of the structure that was used for experimental testing is geometrically nonlinear and highly coupled, there is no closed form solution for active strut adjustments given a required top surface slope (Fest et al. 2003). This fact precludes the use of analytical treatment such as suggested, for example, in Williamson et al. (2003). A single objective stochastic search algorithm (Raphael and Smith 2003) was

¹Structural Engineering Institute, Ecole Polytechnique Fédérale de Lausanne (EPFL), Station 18, 1015 Lausanne, Switzerland. E-mail: bernard.adam@a3.epfl.ch

²Professor, Structural Engineering Institute, Ecole Polytechnique Fédérale de Lausanne (EPFL), Station 18, 1015 Lausanne, Switzerland (corresponding author). E-mail: ian.smith@epfl.ch

Note. Associate Editor: Michael D. Symans. Discussion open until May 1, 2008. Separate discussions must be submitted for individual papers. To extend the closing date by one month, a written request must be filed with the ASCE Managing Editor. The manuscript for this paper was submitted for review and possible publication on April 18, 2006; approved on March 27, 2007. This paper is part of the *Journal of Structural Engineering*, Vol. 133, No. 12, December 1, 2007. ©ASCE, ISSN 0733-9445/2007/12-1752-1761/\$25.00.

selected as the best method to accommodate the exponentially complex generate-test process that is needed to compute control commands (Domer et al. 2003). Domer and Smith (2005) studied the capacity of this structure and its control system to learn in order to decrease the average time necessary to compute a control command. Since the top surface slope of this structure is measured using three sensors and control commands are needed for ten active struts, a unique solution is rarely attainable. Repetitive use of stochastic search to generate several control commands has provided an opportunity for multiobjective control. Adam and Smith (2007) proposed and validated experimentally a multiobjective approach to compute control commands. Since more robust control commands were computed using this approach than with single objective control, the structure was observed to accommodate multiple loading events over its service life. In these studies, it was assumed that the load position and magnitude were known.

Other studies of tensegrity control involve only numerical simulation. Djouadi et al. (1998) described a theoretical scheme to control vibrations of tensegrity systems. Sultan (1999) proposed a formulation of tensegrity active control and illustrated it with the example of an aircraft motion simulator. Skelton et al. (2000) concluded that since only small amounts of energy are needed to change the shape of tensegrity structures, they are advantageous for active control. Kanchanasaratool and Williamson (2002) proposed a dynamic model to study tensegrity feedback shape control. Van de Wijdeven and de Jager (2005) proposed an example of two-dimensional (2D) tensegrity vibration and shape control.

Damage tolerance of tensegrities is a new research area. It is often assumed that local damage would cause a catastrophic collapse. Appropriate topologies have recently been demonstrated to tolerate local damage. Fu (2005) studied the failure modes of tensegrity domes and proposed design methods. Lazopoulos (2005) analytically studied the buckling of a strut in an elastic six-strut and 24-cable tensegrity module and described its post-critical behavior. While these structures are damage tolerant, they do not have capabilities for self-repair.

Self-diagnosis is supported by system identification through model-based diagnosis. System identification involves determining the state of a system as well as values of key parameters through comparisons between predicted and observed responses (Ljung 1999). In structural engineering, this research area is divided into three subareas: damage identification (Park et al. 2005), load identification (Vanlanduit et al. 2005), and structural property identification (Haralampidis et al. 2005). However, most studies have been validated only on simple structures. Only Maeck and DeRoeck (2003) and Logamarsino and Calderini (2005) tested their methodologies on full-scale civil engineering structures. Errors due to measurement precision and modeling assumptions increase the potential for nonunique solutions. Solutions are usually a set of candidate solutions rather than one single solution (Robert-Nicoud et al. 2005). Most of these studies focus on health monitoring tasks that do not extend to control in the situation of partially defined events.

This paper proposes and validates experimentally self-diagnosis and self-repair methodologies for tensegrity active control in situations of partially defined events. Self-diagnosis involves either loading identification or location of damage. Self-diagnosis solutions are as input for shape control and self-repair. Self-repair involves stiffness increases and stress decreases with respect to damage state. The active tensegrity structure that is used for experimental validation is described in the following

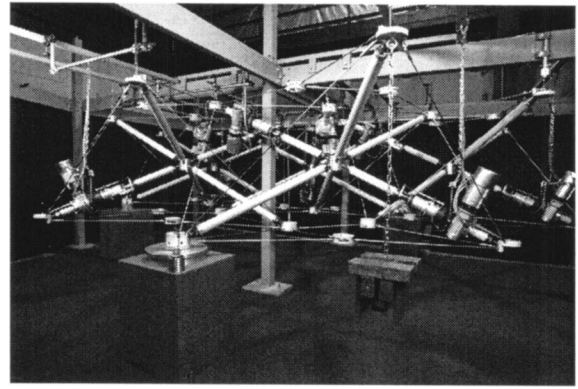


Fig. 1. Five module, 15 m² active tensegrity structure used for tests

section. The following section on self-diagnosis and self-repair describes new methodologies. Results and observations from experimental validation of these proposed methodologies are then discussed. The paper concludes with a discussion of the limitations of these methods, future work, and conclusions.

Description of Structure

The structure is composed of five modules and rests on three supports (Fig. 1). It covers a surface area of 15 m², has a static height of 1.20 m, and withstands a distributed dead load of 300 N/m². It is composed of 30 struts and 120 tendons. Struts are fiber reinforced polymer tubes of 60 mm diameter and 703 mm² cross section. Tendons are stainless steel cables 6 mm in diameter. The central node and star topology is a particularity of each module. This topology was proposed to limit buckling lengths, thereby allowing for more slender compression elements than more traditional tensegrity (Paronesso and Passera 2004). The structure is equipped with an active control system: ten active struts allow for length adjustments and three displacement sensors measure vertical displacements at three nodes of the top surface edge. Shape control involves satisfying a serviceability objective: maintaining the slope of the top surface of the structure when the structure is subjected to a load. The top surface slope is determined through vertical displacement measurements at three nodes: 37, 43, and 48 (Fig. 2). This objective is a control criterion that could be useful for structures such as antennas, pedestrian bridges, and temporary roofs.

Self-Diagnosis

For the purpose of this paper, self-diagnosis involves identifying load positions and magnitudes in situations of partially defined applied loads, and damage location in situations of partially defined damage. Partially defined loading is a known type (for example, single point load), and unknown magnitude and location. Partially defined damage is a known type (for example, a broken cable) and unknown location. Self-diagnosis is supported by system identification. This technique requires neither intensive measurements nor the use of force sensors. The response of the structure to a load and damage is measured and compared to the response of the structure to candidate solutions for load and damage. Three indicators that reflect changes in structure response are used: top surface slope deviation, transversal slope deviation, and

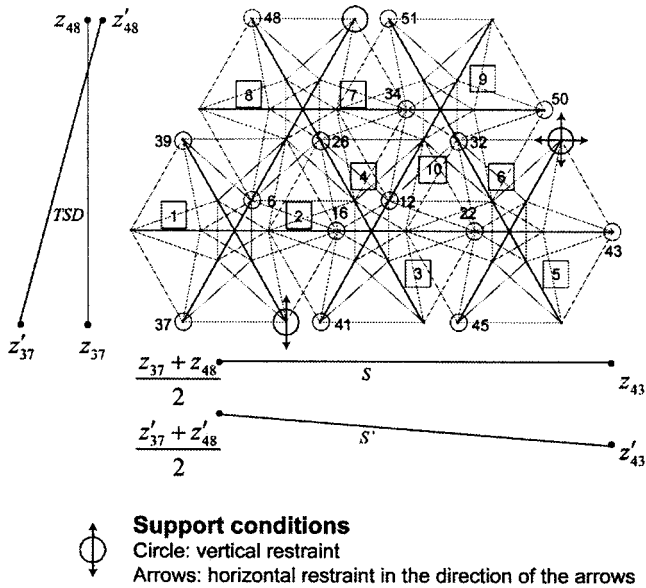


Fig. 2. View of structure from top with ten active struts numbered in squares and upper nodes indicated by circle. Slope S and transversal slope deviation TSD are indicated.

influence vector. These three indicators are presented below:

1. Top surface slope deviation (TSSD): Since maintaining the top surface slope is the main shape control objective, it is also used as the main indicator (Fig. 2)

$$TSSD = \frac{[z'_{43} - (z'_{37} + z'_{48})/2] - [z_{43} - (z_{37} + z_{48})/2]}{L} \quad (1)$$

where z'_i =vertical coordinate of node i after loading and damage event; z_i =vertical coordinate of node i before event; and L =horizontal distance between Node 43 and the middle of segment 37–48 (Fig. 2). $TSSD_m$ is measured on the structure and $TSSD_c$ is calculated through numerical simulation. The slope units used throughout this paper are mm/100 m. Zero top surface slope deviation means that top surface slope is equal to initial top surface slope.

2. The transversal slope deviation (TSD) is introduced in order to evaluate the transversal behavior of the structure (Fig. 2). Its expression is

$$TSD = \frac{1}{L_t} [(z'_{48} - z'_{37}) - (z_{48} - z_{37})] \quad (2)$$

where L_t =transversal distance between Nodes 37 and 48. TSD_m is measured on the structure and TSD_c is calculated through numerical simulation.

3. Top surface slope variations are induced by active control perturbations. They are formally expressed as follows

$$\Delta S = S'' - S'$$

where S'' =top surface slope after active control perturbation and S' =top surface slope before active control perturbation. In the present study, active control perturbations are defined as a 1 mm elongation of active struts (Fig. 2). Top surface slope variations induced by each of the ten active struts are put together in order to create influence vectors \mathbf{v} . The influence vector is the third indicator. These vectors express the top surface slope variation per mm of active strut elongation

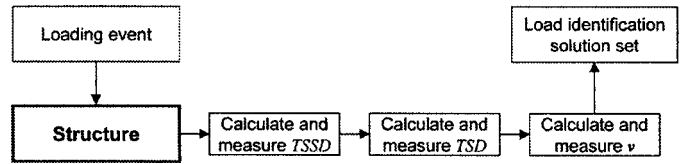


Fig. 3. Indicators involved in load identification process

$$\mathbf{v} = [\Delta S(1) \cdots \Delta S(10)]^T \quad (3)$$

where $\Delta S(i)$ =top surface slope variation per mm of elongation of active strut i . Since tensegrities are self-stressed and flexible structures, they exhibit geometric nonlinear behavior. Active control perturbations are applied through small active strut elongations. Damages and applied loads induce changes in response to active control perturbations. Such changes are measured to support self-diagnosis. Effects are observed through modifications of the influence vector. v_m is measured on the structure and v_c is calculated through numerical simulation.

Load Identification

The load identification involves magnitude evaluation and load location. The methodology uses the three aforementioned indicators (Fig. 3). In this study, loading is assumed to be single static vertical point loads. They are applied one at a time on one of the 15 top surface nodes (Fig. 2).

The following steps lead to load identification:

1. Top surface slope deviation TSSD is the first indicator. Once the structure is loaded, magnitude evaluation involves numerically determining, for each of the 15 top surface nodes, which load magnitude can induce a top surface slope deviation $TSSD_c(Q_j)$ that is close to the one measured on the structure $TSSD_m$. This evaluation is performed iteratively for each node j of the top surface (Fig. 2). Load magnitudes are gradually increased until relation (4) becomes true. Loads are incremented in steps of 50 N

$$TSSD_c(Q_j) > TSSD_m, \quad Q_j = 50, 100, 150, \dots, j = 1, \dots, 15 \quad (4)$$

Value pairs of load magnitudes and locations create a set of candidate solutions. Negative loads (upward) are not considered.

2. Transversal slope deviation TSD is the second indicator. Trends must be the same. Candidate solutions that do not satisfy expression (5) are rejected

$$\frac{TSD_c}{\text{abs}(TSD_c)} = \frac{TSD_m}{\text{abs}(TSD_m)} \quad (5)$$

Experiments show that 2.9 mm/100 m is an upper bound for measurement error of transversal slope deviation. In situations where the absolute value of transversal slope deviation is less than 2.9 mm/100 m, no candidate solution is rejected. This difference between measurements and numerical simulation is related to measurement and modeling errors.

3. The influence vector \mathbf{v} =third indicator. It includes slope variations ΔS per mm of active strut elongations. The influence vector \mathbf{v}_m is evaluated for the structure. Slope variations ΔS_m resulting from active control perturbations are measured. For the remaining candidate solutions, the influence

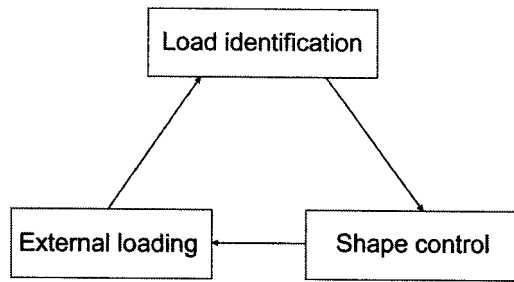


Fig. 4. Load identification and shape control in situations of applied loading

vector \mathbf{v}_c is evaluated through numerical simulation of active control perturbations. The candidate that satisfies expression (6) is taken to be the reference candidate

$$\min|\mathbf{v}_c - \mathbf{v}_m| = \min \left(\sqrt{\sum_{j=1}^{10} (\Delta S_c(j) - \Delta S_m(j))^2} \right) \quad (6)$$

where j indicates the active strut. Practical applications of system identification include consideration of errors. An upper bound for the error on slope variations for one single active control perturbation has been observed to be $e_p=0.11$ mm/100 m. The error e_p =half of the maximum error of slope variation that was observed between top surface slope deviation before and after active control perturbation (+1 mm –1 mm). This error is related to variations in the actuation system and sensor system accuracy. One part of the error between measurements and numerical simulation is taken into account in Eq. (6). Since ten active control perturbations are applied by the ten active struts, candidate solutions that satisfy expression (7) are also taken to be load identification solutions

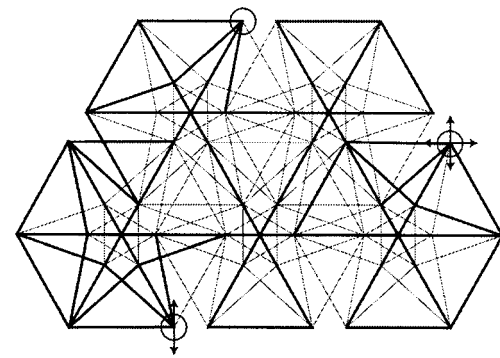
$$|\mathbf{v}_{\text{ref}} - \mathbf{v}_c| \leq 10 \cdot e_p \quad (7)$$

where the subscript ref is introduced to define the reference candidate. This process results in a set of candidate solutions;

- For each of these solutions, load magnitudes are modified to approach more closely measured top surface slope deviation with 10 N increments. Improved candidates create the load identification solution set. In this set, the distance between candidate solution responses and measurements is less than or equal to the maximum error between measurements and numerical simulation. Load identification solutions are used as input to compute a control command for the shape control task (Adam and Smith 2007) (Fig. 4).

Damage Location

Traditional tensegrities do not exhibit redundant load path behavior. Rupture of one single element usually leads to catastrophic collapse. In this structure, module topology and module connections provide redundancy. The basic module contains more cables than the number required to provide stability. Moreover, module connection is provided by multiple cables and nodes. Since loads can follow multiple paths, the structure is redundant and consequently there is potential for tolerating and locating damage. Redundancy is quantified numerically using dynamic relaxation (Barnes 1977). Situations of damage are simulated using dynamic relaxation. Damaged elements leading to structural collapse and progressive collapse through either strut buckling, loss of com-



Support conditions
 Circle: vertical restraint
 Arrows: horizontal restraint in the direction of the arrows

Fig. 5. View of structure from top; critical elements are indicated in bold

pression in a strut (the central node of the structure is stable only through contact compression), or cable ruptures are called critical elements. When subjected to dead load only and for the initial self-stress level, one tenth of cables and the struts are critical elements (Fig. 5). Critical cables are mostly located at the edge of the structure where loads cannot pass through other elements without causing a failure.

In a way similar to the task of load identification, the top surface slope deviation and the influence vector are used as indicators for damage location (Fig. 6). Damage is simulated by removing one cable from the structure. For damage location, a candidate is defined as the structure with one cable removed. The following steps are carried out:

- Top surface slope deviation, TSSD, is the first indicator. Local damage induces top surface slope deviation, TSSD. Top surface slope deviation, $TSSD_m$, is measured on the damaged structure. Since 91 elements are noncritical, 91 candidate solutions are considered. Top surface slope deviation, $TSSD_c$, is numerically simulated for each candidate solution. A maximal error of $e_s=96$ mm/100 m has been observed for simulated values of top surface slope deviation, $TSSD_c$, compared with values of top surface slope deviation, $TSSD_m$, that are measured on the structure for a particular situation of damage. This error is related to model inaccuracies. Candidate solutions are retained in situations where expression (8) is satisfied

$$|TSSD_m - TSSD_c| \leq e_s \quad (8)$$

- The influence vector, \mathbf{v} , is the second indicator. Active control perturbations are numerically simulated for candidate solutions to calculate slope variations, ΔS_c . In situations where instabilities are observed due to active control perturbations, the damage location process stops. However, this phenomenon has not been observed during experimental testing. Ac-

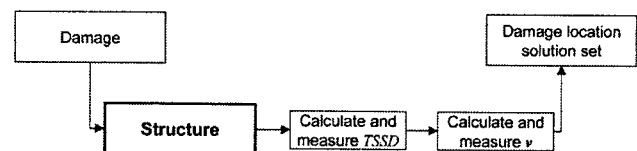


Fig. 6. Indicators involved in damage location process

tive control perturbations are applied to the damaged structure. The candidate with the minimum Euclidian distance between its influence vector \mathbf{v}_c and the influence vector of the damaged structure \mathbf{v}_m is taken to be the reference candidate, according to Eq. (6). Since precision errors are considered, other candidate solutions are taken to be damage location solutions. In situations where expression (7) is satisfied for other candidate solutions, they are also taken to be candidate solutions. The distance between responses of these candidate solutions and reality is less than or equal to the maximum error between measurements and numerical simulation. These solutions are used as input to compute a control command for self-repair.

Self-Repair

In the situation of damage, safety becomes more important than serviceability. Self-repair measures have priority. Therefore, the control objective is modified. The safety objective involves stiffness increases and stress decreases with respect to the damage state. For the purposes of this study, the structure approximate global stiffness indicator is expressed as follows

$$K = \frac{Q_{37} + Q_{43} + Q_{48}}{|\Delta S(Q_{37})| + |\Delta S(Q_{43})| + |\Delta S(Q_{48})|} \quad (9)$$

where $\Delta S(Q_i)$ =top surface slope variation induced by the vertical point load $Q_i=1,000$ N, at node i . Since Q_i is expressed in N and $\Delta S(Q_i)$ in mm/100 m, the approximate global stiffness indicator unit is N/(mm/100 m).

Minimizing stress involves minimizing the normal force in the element of the structure that is the closest to its force capacity. The variable T =maximum force ratio over all cables of the structure

$$T = \max\left(\frac{N}{N_{\text{lim}}}\right) \quad (10)$$

where N =force in cable and N_{lim} =cable force capacity. Previous studies showed that cables are always closer to their capacity than struts. Since stiffness increase and stress decrease are conflicting objectives, a multiobjective search method is attractive to compute control commands that maximize safety. Decision variables are the position of the ten active struts: $\mathbf{x}=(x_1, x_2, \dots, x_{10})$. Objective functions are expressed as follows

$$f_{\text{stress}} = T_c(\mathbf{x}, \mathbf{q}) \quad (11)$$

$$f_{\text{stiffness}} = \frac{1}{K_c(\mathbf{x}, \mathbf{q})} \quad (12)$$

Objective function (11) is the force ratio of the most stressed element. Objective function (12) is the inverse of the global stiffness indicator to avoid too large displacements. Inequality constraints are intended to prevent failure. Constraint functions have the following expressions

$$g_{\text{no_rupture}} = T_c(\mathbf{x}, \mathbf{q}) - 1 \leq 0 \quad (13)$$

$$g_{\text{no_tension}} = \min_{\text{struts}} [N_c(\mathbf{x}, \mathbf{q})] \leq 0 \quad (14)$$

$$g_{x, \text{min}} = -(x_i - x_i^{\text{min}}) \leq 0, \quad \forall i = 1, \dots, 10 \quad (15)$$

Table 1. Load Situations Applied to Structure

Load situation	Loaded node	Load magnitude (N)
1	26	-625
2	26	-900
3	26	-1,209
4	32	-625
5	32	-859
6	32	-1,092
7	37	-550
8	48	-391
9	48	-550
10	48	-700
11	6	-1,092

$$g_{x, \text{max}} = x_i - x_i^{\text{max}} \leq 0, \quad \forall i = 1, \dots, 10 \quad (16)$$

Strut buckling and cable rupture are prevented by constraint (13). Since strut connections are made through contact compression only, tension has to be avoided [Eq. (14)]. Constraints (15) and (16) bound active strut positions. This multiobjective task is summarized as follows

Minimize

$$\{f_{\text{stress}}(\mathbf{x}), f_{\text{stiffness}}(\mathbf{x})\}$$

Subject to

$$g_{\text{no_rupture}}(\mathbf{x}, \mathbf{q})$$

$$g_{\text{no_tension}}(\mathbf{x}, \mathbf{q})$$

$$g_{x, \text{min}}(\mathbf{x})$$

$$g_{x, \text{max}}(\mathbf{x})$$

The proposed methodology for computing self-repairing control commands is based on Pareto filtering in order to avoid the use of weight factors. Sets of Pareto optimal solutions are built according to the stiffness and the stress objectives. Moreover, since multiobjective search supports control command computing, one single solution has to be automatically selected. The slope objective is now of tertiary importance. Among sets of Pareto optimal solutions for stress and stiffness, solutions that exhibit the highest slope compensation are taken to be the solution for the self-repairing control command.

Experimental Testing, Results, and Observations

The proposed methodologies are validated through experimental testing on a full-scale active tensegrity structure (Fig. 1).

Load Identification and Shape Control

The load identification methodology is tested experimentally for 11 loading situations (Table 1). For example, examine loading situation 5 in detail. The structure is loaded with 859 N at Node 32 (Fig. 2).

- Step 1: Top surface slope deviation, TSSD, is the first indicator. The measured slope deviation, $TSSD_m$, is equal to 133.6 mm/100 m. Seven couples of load magnitude and lo-

Table 2. Candidate Solutions for Loading Situation 5: 859 N at Node 32

Candidate	Node	Magnitude (N)	TSSD _c (mm/100 m)	TSD _c (mm/100 m)
1	37	-550	144.1	37.0
2	39	-350	138.6	8.0
3	26	-850	134.6	-2.9
4	32	-800	137.4	-5.1
5	51	-1,050	138.5	-23.1
6	48	-500	134.3	-33.6
7	6	-1,450	135.3	-25.6

Table 3. Slope Variations Measured on Structure for Active Control Perturbation (+1 mm) of Each Active Strut

Active control perturbation	ΔS_m (mm/100m)/mm
1	6.0
2	7.2
3	-9.4
4	-7.4
5	-12.6
6	-12.2
7	9.4
8	9.8
9	-4.3
10	-4.2

cation can induce a top surface slope deviation, TSSD_c, that is close to the one measured according to Eq. (4). The seven candidate solutions are listed in Table 2.

- Step 2: Transversal slope deviation, TSD, is the second indicator. The load on the structure induces a negative transversal slope deviation, TSD_m. Since Candidates 1 and 2 exhibit positive transversal slope deviation, they cannot be solutions and are rejected (Table 2).
- Step 3: The influence vector \mathbf{v} is used as the third indicator. This vector is expressed in terms of the value of slope variation ΔS per mm of active strut elongation. Active control perturbations are applied to the structure by each active strut at a time and slope variations, ΔS_m , are measured. They are presented in Table 3.

Table 4. Slope Variations of Remaining Candidate Solutions for Active Control Perturbation of Each Active Strut

Active control perturbations	ΔS_c (mm/100 m)/mm				
	Candidate 3	Candidate 4	Candidate 5	Candidate 6	Candidate 7
1	9.7	9.9	9.2	10.0	12.0
2	9.7	9.9	9.2	10.0	12.1
3	-4.3	-6.3	-4.5	-5.4	-6.6
4	-4.3	-6.4	-4.5	-5.4	-6.6
5	-11.2	-14.2	-11.6	-13.5	-15.4
6	-11.0	-13.9	-11.3	-13.2	-15.1
7	10.6	11.2	10.2	11.2	13.3
8	10.5	11.2	10.1	11.1	13.2
9	-4.3	-5.4	-3.6	-4.4	-3.9
10	-4.2	-5.2	-3.5	-4.2	-3.7
$ \mathbf{v}_m - \mathbf{v}_c $	7.9	6.7	7.1	7.1	10.6

Table 5. Load Identification Solutions for Load Situation 5: 859 N at Node 32

Candidate	Node	Magnitude (N)	TSSD (mm/100 m)
4	32	-770	132.4
5	51	-1,000	132.9
6	48	-490	131.6

- Step 4: Active control perturbations are numerically simulated on candidate solutions that were not rejected. Slope variations of candidate solutions ΔS_c and Euclidian distance between structure influence vector \mathbf{v}_m and candidate solution influence vectors \mathbf{v}_c are presented in Table 4. Similarity between structure and candidate solutions is maximal when this Euclidian distance is minimal. It is minimal for Candidate 4, 800 N at Node 32, with 6.7 mm/100 m. In other words, in this particular situation, the response to active control perturbations of Candidate 4 is the closest to the response of the structure according to the indicators used. Therefore, Candidate 4 is the reference candidate. Considering precision errors of the active control system, Candidate solutions 5 and 6, 1,050 N at Node 51 and 500 N at Node 48, are also accepted as solutions. The Euclidian distances are both equal to 7.1 mm/100 m.
- Step 5: These three candidate solutions are improved by approaching the measured top surface slope deviation TSSD_m with load magnitude increments of 10 N. The three solutions of load identification are presented in Table 5.

A control command is computed for each of these three load identification solutions using a multiobjective search (Adam and Smith 2007). These three control commands are presented in Table 6. Each of these three control commands is then applied to the structure that is loaded with 859 N at Node 32 for experimental validation. Before applying these control commands to the structure, stresses have to be checked. After simulating control, the maximum compression ranges between 18.4 and 19.1 kN and the maximum tension between 7.9 and 8.1 kN depending on the load identification solution. In Fig. 7, top surface slope deviation is plotted in vertical axis versus steps of 1 mm of active strut adjustments in the horizontal axis. Top surface slope deviation is zero when the top surface slope is equal to the initial slope.

Top surface slope compensation is rarely equal to 100%. For

Table 6. Control Commands for Load Identification Solutions 770 N at Node 32, 1,000 N at Node 51, 490 N at Node 48. Structure Is Loaded with 859 N at Node 32.

Load identification	Travel of the ten active struts (mm)									
	1	2	3	4	5	6	7	8	9	10
770 N at Node 32	-1.99	-1.97	1.45	1.26	1.61	1.63	-1.01	-0.04	1.63	2.00
1,000 N at Node 51	-1.77	-1.87	1.85	1.03	1.93	1.99	-1.78	-2.00	1.01	0.71
490 N at Node 48	-1.85	-2.00	1.65	1.13	2.00	1.00	-0.30	-1.63	0.68	2.00

this loading situation, it ranges between 98 and 104%. These results are summarized in Table 7. To generalize these results, load location and control command computation is carried out for the 11 load situations (Table 1). Load identification solutions are used as input for control command computation. Results in terms of top surface slope compensation error and sequence length are summarized in Table 8. Sequence length is the sum of active strut adjustments in mm.

For load identification, the following observations demonstrate the validity of examining a set of solutions instead of the best solution with respect to a particular indicator:

- a Exact load magnitude and location may not be identified;
- b The distance between load identification solutions and reality is less than or equal to the error between measurements and numerical simulation, according to the indicators;
- c The reference candidate is not always the one that is located at the same node as the applied load situation; and
- d When Node 6 is loaded with 1,092 N, load identification solutions do not contain Node 6. The error evaluation might be improved in order to identify Node 6.

Another observation also emerges: geometrical nonlinear behavior of tensegrity structures is represented through influence vector changes with respect to load magnitude and location. The influence vector depends upon the self-stress state.

The following observations demonstrate the validity of using load identification to improve shape control. While the average error of slope compensation was equal to 16.6% when load identification was not used, it improves down to 9.4% when using load identification solutions to compute control commands. Similarly, the maximum error of slope compensation improves from 41.6 to 27%. Slope compensation improves when using load identification solutions to compute control commands, since the distance between load identification solutions and reality is less than the error between measurements and numerical simulation. The following observations are also made on the basis of these results:

1. In each of these sets, the maximum difference between the worst and the best top surface slope compensation is less than 15%.
2. The exact load location does not always lead to the best top surface slope compensation.
3. The reference candidate, defined as the self-diagnosis candidate solution for which Euclidian distance is minimum with the real structure, does not always lead to the best top surface slope compensation.

Damage Location

Cable 128 was removed from the structure to simulate a damage situation. Damage location involves two steps.

1. Top surface slope deviation $TSSD_m$ is equal to $-105 \text{ mm}/100 \text{ m}$. Three candidate solutions induce a $TSSD_c$

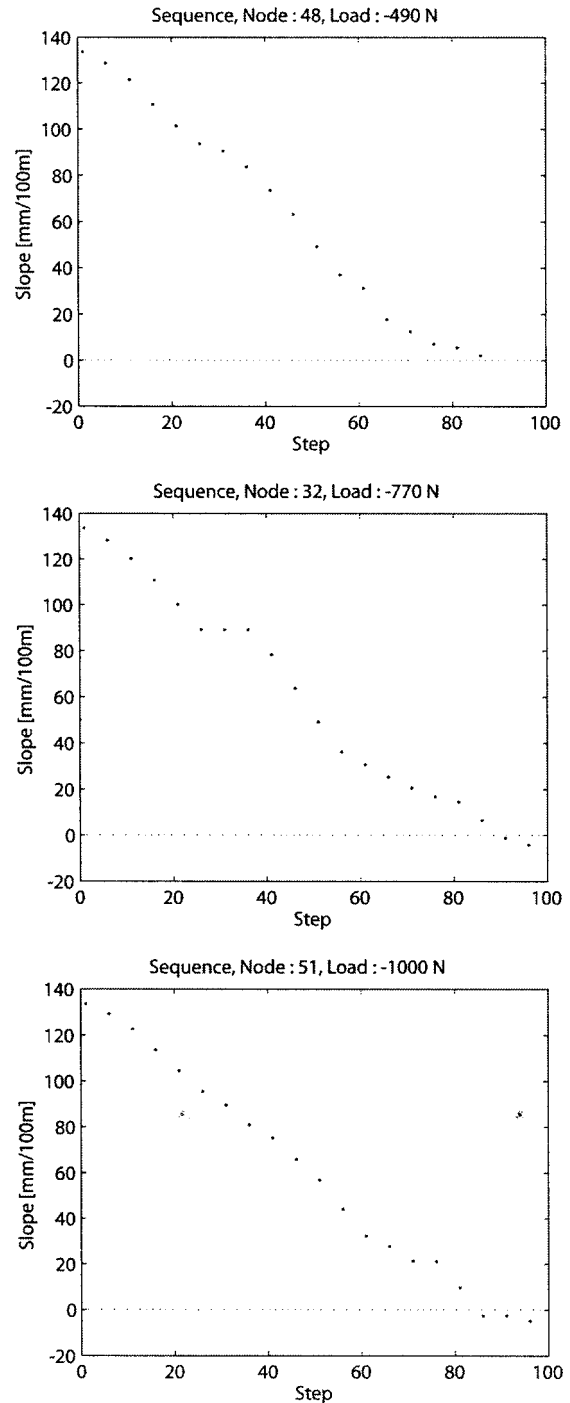


Fig. 7. Shape control for load situation 5: 859 N at Node 32, for the three load identification solutions: 770 N at Node 32, 1,000 N at Node 51, and 490 N at Node 48

Table 7. Top Surface Slope Compensation SC_m when Structure Is Controlled with Control Commands Using Load Identification Solutions as Input

Load identification solution	SC_m (%)	e_{sc} (%)
770 N at Node 32	103	3
1,000 N at Node 51	104	4
490 N at Node 48	98	2

that is close to this value, according to Eq. (8). These candidates are listed in Table 9; and

- Influence vector \mathbf{v} =second indicator. Slope variations ΔS_c due to active control perturbations are numerically simulated on the three remaining candidate solutions: cables 42, 121, and 128 broken.

Slope variation values are presented in Table 10. Slope variations, ΔS_m , are measured on the structure and listed in Table 11. The Euclidian distance is the least for Candidates 3, cable 128 broken

Table 8. Summary of Load Identification Solutions and Shape Control Results

Load situation		Load identification solution		Shape control			
Loaded node	Load magnitude (N)	Loaded node	Load magnitude (N)	e_{sc} (%)	Sequence length (mm)		
26	-625	51	-540	17	17.1		
		26	-470	11	18.1		
		39	-190	2	18.1		
		37	-290	5	20.3		
		48	-280	6	13.2		
26	-900	51	-730	10	14.7		
		26	-620	0	19.8		
26	-1,209	51	-1,010	7	18.7		
		26	-850	6	19.9		
32	-625	39	-270	12	21.0		
		51	-780	18	15.9		
		32	-620	8	16.6		
		37	-410	9	18.6		
		48	-400	4	16.3		
		26	-660	6	15.5		
		32	-859	32	-770	3	14.6
		51	-1,000	4	15.9		
32	-1,092	48	-490	2	14.3		
		32	-980	3	18.6		
37	-550	48	-620	1	18.4		
		39	-350	26	17.7		
48	-391	37	-530	27	16.3		
		51	-700	5	13.0		
		48	-360	12	15.4		
48	-550	26	-600	6	17.0		
		32	-560	20	17.9		
		48	-510	6	16.9		
48	-700	32	-810	11	13.1		
		48	-660	12	20.0		
6	-1,092	32	-1,050	15	21.2		
		32	-610	16	13.9		
		48	-390	11	16.1		

Table 9. Candidate Solutions That Induce $TSSD_c$ Close to $TSSD_m$ according to Eq. (8)

Candidate	Broken cable	$TSSD_c$ (mm/100 m)
1	42	-122
2	121	-102
3	128	-102

with a value of 12.6 mm/100 m. It is taken to be the reference candidate. According to Eq. (7), no other candidate solution is accepted since Euclidian distance is equal to 20.3 mm/100 m and 14.9 mm/100 m for Candidate 1 (cable 43 broken) and Candidate 2 (cable 121 broken).

Self-Repair

As described earlier, self-repair involves increasing stiffness and decreasing the stresses with respect to the damage state. Examine the self-repair process when cable 128 is removed from the structure. Damage location solution is exact in this situation. Fig. 8 illustrates global stiffness indicator and force ratio evolution during damage and self-repair.

In the initial state, the global stiffness indicator K_c is equal to 3.7 N/mm/100 m and maximal tension in cable elements T_c is equal to 7.78 kN. When cable 128 is removed, the global stiffness indicator falls down to 3.3 N/mm/100 m and highest tension increases to 7.83 kN. When the self-repairing control command is applied, the global stiffness indicator increases to 3.4 N/mm/100 m and the highest tension decreases to 7.76 kN. For the purposes of this example, stiffness indicator and stress values are numerical values. The following observations are of interest:

- The possibility of controlling objectives such as stiffness and stress by modifying the self-stress state of an active tensegrity structure is demonstrated.
- The topology of the tensegrity structure in this study allows for redundant load-path behavior for some types of damage.

Limitations and Future Work

While the self-diagnosis algorithm that is presented in this paper is able to identify only single loads, a generalization of this algo-

Table 10. Influence Vector and Euclidian Distance for Remaining Candidates Listed in Table 9

Active control perturbation	ΔS_c (mm/100 m)/mm		
	Candidate 1	Candidate 2	Candidate 3
1	10.04	11.33	10.43
2	10.06	11.32	10.42
3	-14.18	-11.14	-2.35
4	-13.85	-11.14	-2.41
5	-12.38	-8.84	-13.96
6	-12.15	-8.73	-13.78
7	18.73	5.19	9.80
8	18.88	4.97	9.70
9	-0.97	0.37	-12.05
10	-0.88	0.58	-11.86

Table 11. Influence Vector Values for Damaged Structure

Active control perturbation	ΔS_m (mm/100 m)/mm
1	6.72
2	8.16
3	-4.08
4	-4.32
5	-11.75
6	-11.27
7	8.88
8	9.59
9	-4.08
10	-4.32

rithm to more complex loading and damage patterns as well as more complex structures is possible. More complex loading damage and structures lead to larger solution spaces for self-diagnosis. Stochastic search is practicable and efficient in situations where a global minimum has to be found in combinatorial large solution spaces. Consequently, stochastic search could be implemented in the self-diagnosis methodology that is presented in this paper to generate and filter more complex candidate solutions. More parameters could be taken into account. The use of variables such as number of point loads, load locations, load directions, load magnitudes, types of damage, damage locations, and characteristics of the elements would result in more accurate self-diagnosis solutions for more complex structures. This would also allow for an extension of self-diagnosis to be usable over scenarios of multiple loading events and damage.

Since tensegrities are lightweight structures, they are susceptible to vibrations. In practical situations, civil engineering structures are subjected to mechanical, pedestrian, traffic, wind, and earthquake loading and in addition, space structures could be subjected to rapid temperature changes and impact due to debris. In situations where an excitation frequency is close to natural frequencies, the structure could resonate. Current work includes a study of the effect of vibrations and the capacity of the active control system to attenuate them.

Conclusions

Self-diagnosis, including load identification and damage location, does not always identify exact loading situation and exact damage locations. Nevertheless, inexact solutions are closer to reality than the maximum error between measurements and numerical simulation. Compared with computations from exact loading, shape control even improves when control commands are computed from load identification solutions. Self-diagnosis methodologies are particularly attractive for active control in situations where there may be partially defined applied loading and damage.

In the event of damage, safety becomes more important than serviceability. The conclusions from the study on self-repair are summarized below:

1. Self-repair has the potential to be supported by active control systems for active structures.
2. Potential for self-repair that increase stiffness and decrease stresses with respect to the damaged state is demonstrated. However, self-repair is a qualified success, since 100% of the damage is not compensated.
3. When the damage location solution is exact, self-repair is

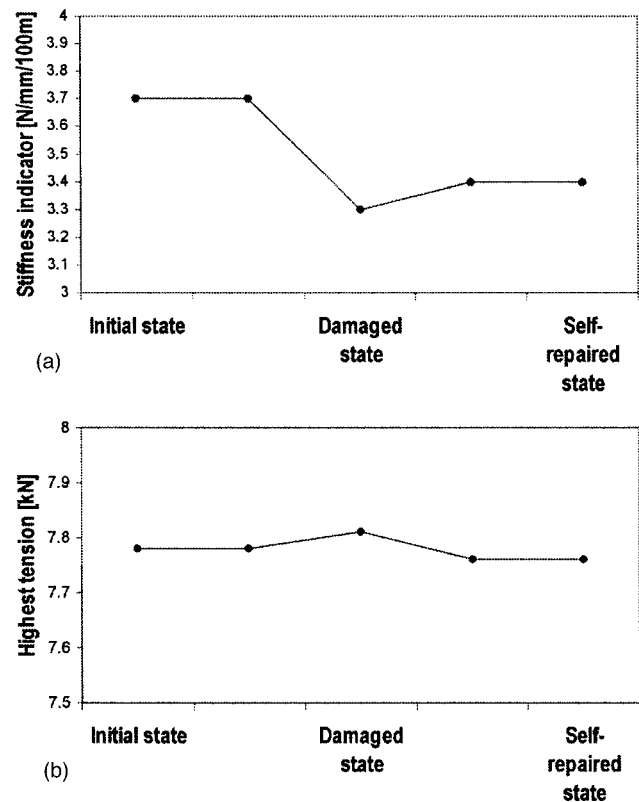


Fig. 8. Evolution of global stiffness indicator: (a) and highest tension; (b) during damage of cable 128 and self-repair

attractive for active structures in situations of partially defined damage.

4. When damage location is not exact, self-repair might lead to stress increase. Additional information, for example stress measurements, would be useful to improve damage location. Therefore, the methodologies described in this paper are attractive for active control in situations where there may be unanticipated applied loading and damage.

Acknowledgments

The writers would like to thank the Swiss National Foundation for supporting this work. They also thank B. Domer, P. Kripakaran, and B. Rebora for discussions and advice. B. Domer also improved control and implemented the case-based reasoning study. E. Fest built the structure and the control system. B. Raphael provided support during programming of the control system. They are also grateful to Y. Robert-Nicoud for his advice, Passera & Pedretti SA (Lugano, Switzerland), Lust-Tec GmbH (Zürich, Switzerland), and P. Gally for their contributions.

Notation

The following symbols are used in this paper:

e_p = upper bound error on top surface slope variation for one single active control perturbation, between structure and numerical models;

e_s = upper bound error on top surface slope deviation between structure and numerical models due to damage;
 K = global stiffness indicator;
 L = horizontal distance between Node 43 and middle of segment 37–48;
 N = normal force;
 N_{lim} = normal force capacity;
 R = transversal slope deviation;
 S = top surface slope deviation;
 S' = slope deviation before active control perturbation;
 S'' = slope deviation after active control perturbation;
 T = ratio between normal force and normal force capacity for element that is closest to its capacity;
 \mathbf{v} = influence vector;
 \mathbf{v}_{can} = influence vector of candidate;
 \mathbf{v}_{ref} = influence vector of reference candidate;
 z_i = vertical coordinate of node i , at initial state;
 z'_i = vertical coordinate of node i , after partially defined event occurrence;
 ΔS = top surface slope variation; and
 ΔS_{can} = numerically calculated top surface slope variation of candidate for active control perturbation.

References

- Adam, B., and Smith, I. F. C. (2007). "Tensegrity active control: Multi-objective approach." *J. Comput. Civ. Eng.*, 21(1), 3–10.
- Averseng, J., and Crosnier, B. (2004). "Static and dynamic robust control of tensegrity systems." *J. Int. Asso. for Shell and Spatial Struct.*, 45, 169–174.
- Barnes, M. R. (1977). "Form finding and analysis of tensioned space structures by dynamic relaxation." Ph.D. thesis, The City Univ. of London, London.
- Djouadi, S., Motro, R., Pons, J. C., and Crosnier, B. (1998). "Active control of tensegrity systems." *J. Aerosp. Eng.*, 11(2), 37–44.
- Domer, B., Raphael, B., Shea, K., and Smith, I. F. C. (2003). "A study of two stochastic search methods for structural control." *J. Comput. Civ. Eng.*, 17(3), 132–141.
- Domer, B., and Smith, I. F. C. (2005). "An active structure that learns." *J. Comput. Civ. Eng.*, 19(1), 16–24.
- Fest, E., Shea, K., Domer, B., and Smith, I. F. C. (2003). "Adjustable tensegrity structure." *J. Struct. Eng.*, 129(4), 515–526.
- Fest, E., Shea, K., and Smith, I. F. C. (2004). "Active tensegrity structure." *J. Struct. Eng.*, 130(10), 1454–1465.
- Fu, F. (2005). "Structural behavior and design methods of tensegrity domes." *J. Constr. Steel Res.*, 61, 23–35.
- Haralampidis, Y., Papadimitriou, C., and Pavlidou, M. (2005). "Multiobjective framework for structural model identification." *Earthquake Eng. Struct. Dyn.*, 34, 665–685.
- Kanchanasaratool, N., and Williamson, D. (2002). "Modelling and control of class NSP tensegrity structures." *Int. J. Control*, 75(2), 123–139.
- Kawaguchi, K., Pellegrino, S., and Furuya, H. (1996). "Shape and stress control analysis of prestressed truss structures." *J. Reinf. Plast. Compos.*, 15, 1226–1236.
- Lagomarsino, S., and Calderini, C. (2005). "The dynamical identification of the tensile force in ancient tie-rods." *Eng. Struct.*, 27, 846–856.
- Lazopoulos, K. A. (2005). "Stability of an elastic cytoskeletal tensegrity model." *Int. J. Solids Struct.*, 42, 3459–3459.
- Ljung, L. (1999). *System identification-theory for the users*, Prentice-Hall, Englewood Cliff, N.J.
- Maeck, J., and De Roeck, G. (2003). "Damage assessment using vibration analysis on the z24-bridge." *Mech. Syst. Signal Process.*, 17, 133–142.
- Motro, R. (1984). "Forms and forces in tensegrity systems." *Proc., 3rd Int. Conf. on Space Structures*, H. Nooshil, ed., Elsevier, Amsterdam, The Netherlands, 180–185.
- Motro, R. (2003). *Tensegrity: Structural systems for the future*, Hermes, ed., Penton Science, London.
- Park, G., Rutherford, A. C., Sohn, H., and Farrar, C. R. (2005). "An outlier analysis framework impedance-based structural health monitoring." *J. Sound Vib.*, 286, 229–250.
- Paronesso, A., and Passera, R. (2004). "The cloud of Yverdon." *Proc., IASS 2004 Symp., International Association for Shell and Spatial Structures* (CD-ROM), Editions de l'Espérou, Montpellier, France.
- Pawlowski, P., and Holnicki-Szulc, J. (2004). "Adaptive structures under extreme loads—Impact detection, self-adaptation, self-repairing." *Proc., 3rd European Conf. on Structural Control*, Vienna, Austria.
- Raphael, B., and Smith, I. F. C. (2003). "A direct stochastic algorithm for global search." *Appl. Math. Comput.*, 146(2–3), 729–758.
- Robert-Nicoud, Y., Raphael, B., and Smith, I. F. C. (2005). "System identification through model composition and stochastic search." *J. Comput. Civ. Eng.*, 19(3), 239–247.
- Shea, K., Fest, E., and Smith, I. F. C. (2002). "Developing intelligent tensegrity structures with stochastic search." *Adv. Eng. Inf.*, 16(1), 21–40.
- Skelton, R. E., Helton, J. W., Adhikari, R., Pinaud, J. P., and Chan, W. (2000). "An introduction to the mechanics of tensegrity structures." *Handbook on mechanical systems design*, CRC, Boca Raton, Fla.
- Sobek, W., and Teuffel, P. (2002). "Adaptive lightweight structures." *Proc., International IASS Symp.*, Warsaw, Poland, J. B. Obrebski, ed., Micro Publisher, Wydawnictwo Naukowe, Poland, 203–210.
- Sterritt, R., Parashar, M., Tianfield, H., and Unland, R. (2005). "A concise introduction to autonomic computing." *Adv. Eng. Inf.*, 19, 181–187.
- Sultan, C. (1999). "Modeling, design and control of tensegrity structures with applications." Ph.D. thesis, Purdue Univ., West Lafayette, Ind.
- Teuscher, C., Mange, D., Stauffer, A., and Tempesti, G. (2003). "Bioinspired computing tissues: Towards machine that evolve, grow, and learn." *BioSystems*, 68, 235–244.
- Van de Wijdeven, J., and de Jager, B. (2005). "Shape change of tensegrity structures: Design and control." *Proc., American Control Conf.*, Portland, Ore., 2522–2527.
- Vanlanduit, S., Guillaume, P., Cauberghe, B., Parloo, E., De Sitter, G., and Verboven, P. (2005). "Online identification of operational loads using exogenous inputs." *J. Sound Vib.*, 285, 267–279.
- Von Neumann, J. (1966). *The theory of self-reproducing automata*, University of Illinois Press, Urbana, Ill.
- Williamson, D., Skelton, R. E., and Han, J. (2003). "Equilibrium conditions of a tensegrity structure." *Int. J. Solids Struct.*, 40, 6347–6367.